Tomographic Images of Blood Pool and Perfusion in Brain and Heart

Michael E. Phelps, Edward J. Hoffman,* R. Edward Coleman, Michael J. Welch, Marcus E. Raichle, Edward S. Weiss, Burton E. Sobel, and Michel M. Ter-Pogossian

Mallinckrodt Institute of Radiology and Washington University School of Medicine, St. Louis, Missouri

A whole-body positron-emission transaxial tomograph (PETT III) was used to image the cross-sectional distribution of $^{13}NH_3$ and ^{11}CO-hemoglobin in the human brain and heart. Carotid and intravenous bolus injections of $^{13}NH_3$ in the rhesus monkey had shown that $^{13}NH_3$ is efficiently extracted by the brain and clears from it slowly (half-time, 40–50 min for carotid injections and 60–70 min for intravenous injections). The intravenous tomographic images in humans showed an excellent relationship between $^{13}NH_3$ uptakes in the cortex, subcortical white matter, cerebellum, and brain stem and normal blood perfusion or flow in these structures. Cerebral lesions with high (metastasis) and low (stroke) blood flows showed correspondingly high and low uptakes of $^{13}NH_3$. Large- and small-vascular structures of the brain were also clearly seen in ^{11}CO-hemoglobin tomographic images. Normal myocardium and the ventricular chambers were well defined, and a transmural anterior myocardial infarct was clearly shown. The effective combination of positron transaxial tomography and compounds labeled with positron-emitters provides a safe new method for quantitatively imaging hemodynamic and physiologic functions of selected organs with good tomographic image quality.

A wide variety of in vivo tracer techniques has been used to measure cerebral and cardiac hemodynamics. Radioactive inert gases, such as ^{85}Kr and ^{133}Xe, and other radioactive compounds, such as $H_2^{15}O$ or ^{131}I-antipyrine, have been used as diffusible tracers to determine organ blood flow by applying the formulations developed by Zierler (*1*). Tracers have been employed to label plasma and red blood cells for the direct (*1*) or indirect measurement of vascular transit time or blood distribution.

Other techniques have measured blood flow by the extraction and retention of tracers by perfused tissue, or by the retention in capillaries or arterioles of labeled microspheres or other particulate matter. The former approaches have essentially employed principles developed by Saperstein (*2*) and are exemplified by the cardiac studies using radioisotopes of K, Cs, and Rb and the compound $^{13}NH_3$. The latter, capillary-retention approach frequently employs ^{99m}Tc-labeled particles or macroaggregated albumin to determine flow distribution from active trapping, e.g., by the reticuloendothelial cells or simply by capillary occlusion.

The poor spatial resolution or qualitative nature of conventional in vivo detection techniques has severely restricted the amount of clinically useful information obtained from these studies. These limitations can be avoided by the effective combination of transaxial reconstruction radionuclide tomography (*3–5*) and static distribution models of blood flow (e.g., Saperstein's approach) or blood volume.

Nitrogen-13-ammonia has been used for imaging the myocardium by Harper et al (6,7) with a scintillation camera and by Monahan et al (8) with a rectilinear scanner. These studies show the feasibility of using $^{13}NH_3$ as a myocardial-imaging agent for normal or infarcted myocardium. However, image quality was severely limited by the detection systems employed. Hoop et al (9,10) and Brownell et al (11) have obtained better-quality images using the Massachusetts General Hospital positron camera with $^{13}NH_3$ for imaging the heart (9,11) and with $^{13}NH_3$ and $C^{15}O_2$ for imaging the brain (10,11). These authors suggest that the CO_2 images may reflect bloodflow distributions. In these studies the same positron camera was used for either focal-plane or transaxial tomography. Transaxial tomographic studies with $^{13}NH_3$ in dogs (9,11) have shown good differentiation between infarcted and normal myocardium. Using the Massachusetts General Hospital positron camera for myocardial imaging in the dog, Budinger et al (12) showed that comparable image quality can be obtained with $^{13}NH_3$ and with ^{82}Rb delivered by a ^{82}Sr generator system. Carter et al (13) also used $^{13}NH_3$ to evaluate the effect of blood pH and blood NH_3 concentration on $^{13}NH_3$ uptake in the liver and brain of dogs.

Kuhl et al (4), using the Mark-III scanner and ^{99m}Tc-labeled red blood cells, have quantitatively imaged the cross-sectional blood volume in human subjects and monkeys. Recently this group has also investigated ^{123}I-antipyrine as a diffusible tracer for the cross-sectional imaging of cerebral perfusion (14). Budinger et al (15) have investigated the use of ^{201}Tl and ^{131}Cs for transaxial tomographic imaging of the heart with a scintillation camera.

Our previous studies with a prototype positron-emission transaxial tomograph, PETT (3,16,17), and a whole-body system for human studies, PETT III (3,18–24), have shown the high resolution, contrast, quantitative accuracy, and potential application of this technique for imaging hemodynamic and metabolic processes in the brain, heart, kidneys, and liver. The present work describes the relationship between perfusion and $^{13}NH_3$ accumulation in cerebral and myocardial tissue. It also illustrates the image quality of PETT III for cross-sectional imaging of blood pools and perfusion with $^{13}NH_3$ and ^{11}CO.

MATERIALS AND METHODS

Preparation of $^{13}NH_3$, ^{11}CO, and ^{68}Ga. Nitrogen-13 is produced in the Washington University Medical Cyclotron by a $^{12}C(d,n)^{13}N$ reaction in which methane gas is the target, using an adaptation of the method first described by Tilbury et al (25). The

$^{13}NH_3$ formed was collected with a gas-circulating system and trapped in an acidic water solution. After this solution was made basic, the $^{13}NH_3$ was distilled into a slightly acidic saline solution which was then passed through a Millipore filter. The $^{13}NH_3$ preparation was carried out under sterile pyrogen-free conditions. The radiochemical purity, as determined by gas–liquid chromatography, was typically 97% $^{13}NH_3$, 0.3% $CH_3^{13}NH_2$, and 2% unknown (26).

The ^{11}CO is produced by the $^{10}B(d,n)^{11}C$ reaction in a boric oxide target. The resulting mixture of gaseous ^{11}CO and $^{11}CO_2$ is swept out of the target chamber and passed over zinc at 700°C to reduce the $^{11}CO_2$ to ^{11}CO. The ^{11}CO gas is then collected in an ambu bag for administration to the subject by inhalation.

The ^{68}Ga is obtained from a New England Nuclear ^{68}Ge generator. The ^{68}Ga is eluted from the generator and used in the form of ^{68}Ga-EDTA (0.05 M EDTA).

Animal studies. Adult rhesus monkeys whose external carotid arteries had been ligated 2–3 weeks previously were used to measure the extraction of $^{13}NH_3$ by cerebral tissues. The monkeys were anesthetized with phencyclidine HCl and given atropine. They were paralyzed with gallamine triethiodide and passively ventilated on 100% oxygen with a Harvard respirator. A 0.2-cm^3 bolus of $^{13}NH_3$, ^{133}Xe dissolved in saline, or ^{11}CO-hemoglobin was injected into the internal carotid artery through a catheter introduced through a femoral artery. The ^{133}Xe and ^{11}CO-hemoglobin were used for the measure of cerebral blood flow and vascular mean transit time, respectively (27,28). Catheters, placed in the right and left femoral veins, was used for intravenous injection of $^{13}NH_3$ and also for an external loop through which activity in the circulating blood could be monitored with a shielded NaI(Tl) detector.

Another shielded and collimated NaI(Tl) detector was placed under the monkey's head to record the time course of the injected activity in the brain. The data were collected, processed, and displayed by an on-line minicomputer (27).

Human studies. Transaxial tomographic scans of the head and chest were performed following either the intravenous administration of $^{13}NH_3$ or the inhalation of ^{11}CO. These scans were performed with the PETT III, the basic principles (3,16,17), design, and performance characteristics of which have been presented previously (3,18–21,24). The subject, placed on a movable bed, was positioned in the tomograph at the cross-sectional level of interest with the aid of a low-power laser beam of light across the center plane of the tomograph. After
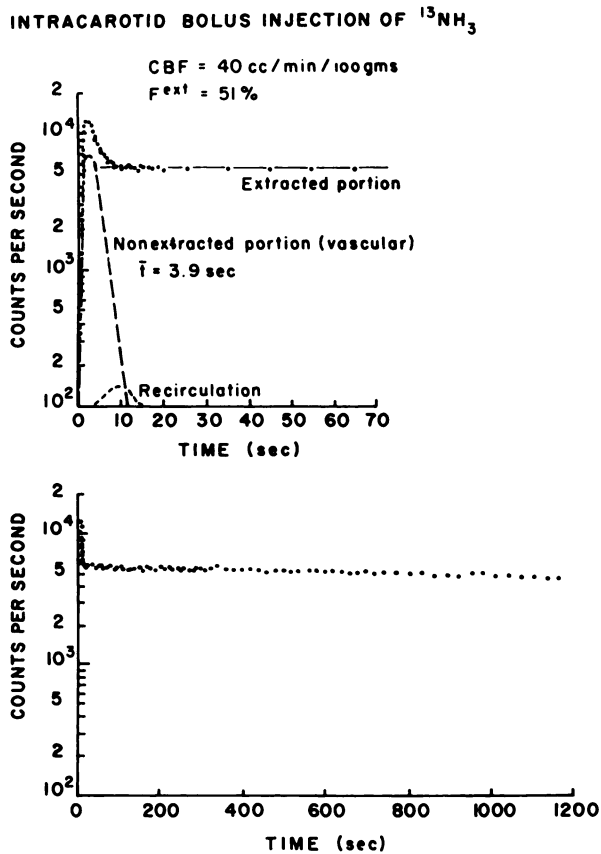
INTRACAROTID BOLUS INJECTION OF ^{13}NH$_3$

CBF = 40 cc/min/100 gms
F^{ext} = 51%

FIG. 1. Time—activity curve from brain after intracarotid injection of ^{13}NH$_3$ in rhesus monkey. (Top) 70-sec plot analyzed into individual components of ^{13}NH$_3$ extracted into tissue, nonextracted portion, and recirculated portion. (Bottom) 1200-sec plot showing retention and slow clearance of extracted ^{13}NH$_3$.

injecting 10–15 mCi of ^{13}NH$_3$ intravenously, 4–5 min were allowed for equilibration and extraction by the tissues, and then data for the first slice were collected for 4–5 min. Generally, 3–5 cross-sectional slices were examined sequentially. The data-collection time was progressively increased for each slice to compensate for radioactive decay. Thus, the data-collection time of the last slice was usually about 12 min. The total number of counts per image ranged from 4 × 10^5 to 1.5 × 10^6. About 40 min after the end of the ^{13}NH$_3$ study was allowed for the decay of ^{13}N activity. The subject then breathed 10–15 mCi of ^{11}CO in an ambu bag for approximately 30 sec to label the blood with ^{11}CO-hemoglobin. The data-collection sequence was then repeated.

Several patients with cerebral lesions were injected intravenously with about 3 mCi of ^{68}Ga-EDTA. After 0.5 hr to allow for clearance from the blood, 12-min scans were performed.

The control of the linear and angular scanning motion and data collection, processing, and display in PETT III are performed by an on-line minicomputer.

The collected data are corrected for photon attenuation either by viewing an external source of positron activity through the examined cross section or by using the average attenuation coefficient and the geometric shape of the cross section (3,16). The former method was used for the chest and the latter for the head. The accuracy of these techniques has been presented previously for human subjects (18).

The spatial resolution of PETT III can be varied by simply changing a small lead shield in front of the detectors. A FWHM system resolution (24) of either 1.3 or 2.2 cm was employed in all the studies presented here. A 3° angular and 1- or 0.5-cm linear sampling resolution were employed. Finally, the images were reconstructed with a convolution-based algorithm and displayed in a 100 × 100 matrix. No subsequent image processing was employed.

RESULTS AND DISCUSSION

Brain. Carotid bolus injections of ^{13}NH$_3$ in the rhesus monkey were performed to examine the single-pass extraction of ^{13}NH$_3$ by cerebral tissue in order to better understand the data from the intravenous procedure employed in the tomographic studies. Figure 1 shows a typical time–activity curve from an intracarotid ^{13}NH$_3$ injection at a cerebral blood flow (CBF) of 40 cm^3/min/100 gm (the CBF was measured with ^{133}Xe). The 70-sec plot was analyzed into the extracted portion of ^{13}NH$_3$ which passes from the blood and is retained by the cerebral tissue (plateau), the vascular or nonextracted portion of ^{13}NH$_3$ which remains in the blood and passes through the brain, and then a small component (less than 2%) which is recirculated. The mean transit time of the vascular component of the ^{13}NH$_3$ curve was 3.9 sec, which agrees well with the vascular mean transit time of 4 sec measured subsequently with ^{11}CO-hemoglobin. The fraction of ^{13}NH$_3$ extracted into the tissue (about 50%) had a washout half-time from the tissue of about 45 min.

The ^{13}N-ammonia in the injected solution is in equilibrium with un-ionized ammonia ^{13}NH$_3$ and ammonium ion ^{13}NH$_4$$^+$. At the normal blood pH of 7.4, only about 3% is in the form of ^{13}NH$_3$, the only form that will diffuse freely through the blood–brain barrier. However, as ^{13}NH$_3$ leaves the blood, it is immediately replenished by the chemical conversion of ^{13}NH$_4$$^+$ into ^{13}NH$_3$. For example, if the ^{13}NH$_3$ ⇌ ^{13}NH$_4$$^+$ equilibrium is upset, one can determine from the forward and reverse rate constants (29) that it takes about 19 μsec to return to equilibrium. Thus, ^{13}NH$_3$ acts like a diffusible tracer without hindrance from the large portion in the form of ^{13}NH$_4$$^+$. As shown in Fig. 2, the ^{13}NH$_3$ that crosses the blood–brain barrier equilibrates with the extra-
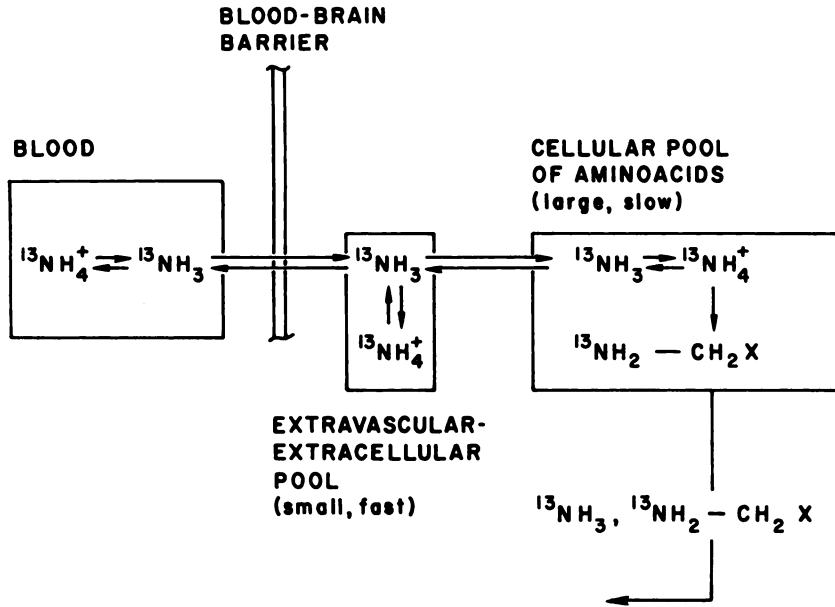
FIG. 2. Compartmental distribution of $^{13}NH_3$ extraction from blood into brain tissue, retention in amino acid pools in tissue, and clearance of ^{13}N activity from tissue as ammonia and amino acids.

vascular–extracellular ammonia pool and is rapidly incorporated into the amino acid metabolism. The small pool of free ammonia in the brain is reported to turn over 75% per second (30). The long half-time ($\sim$ 40–50 min) of the plateau in Fig. 1 probably results from the fact that the $^{13}NH_3$ is incorporated in the large pool of amino acids and leaves the brain tissue at a very slow rate as labeled amino acids and free $^{13}NH_3$.

Time–activity curves from the brain and circulating blood after an intravenous injection of $^{13}NH_3$ are shown in Fig. 3. The cerebral curve is similar to that for the carotid study except that the plateau region continues to increase slightly for the first 300 sec and then remains flat up to 700–800 sec; from 800 sec on (not shown), the curve slowly decreases with a half-time of 70–80 min. This difference between the intravenous bolus and the carotid proce-
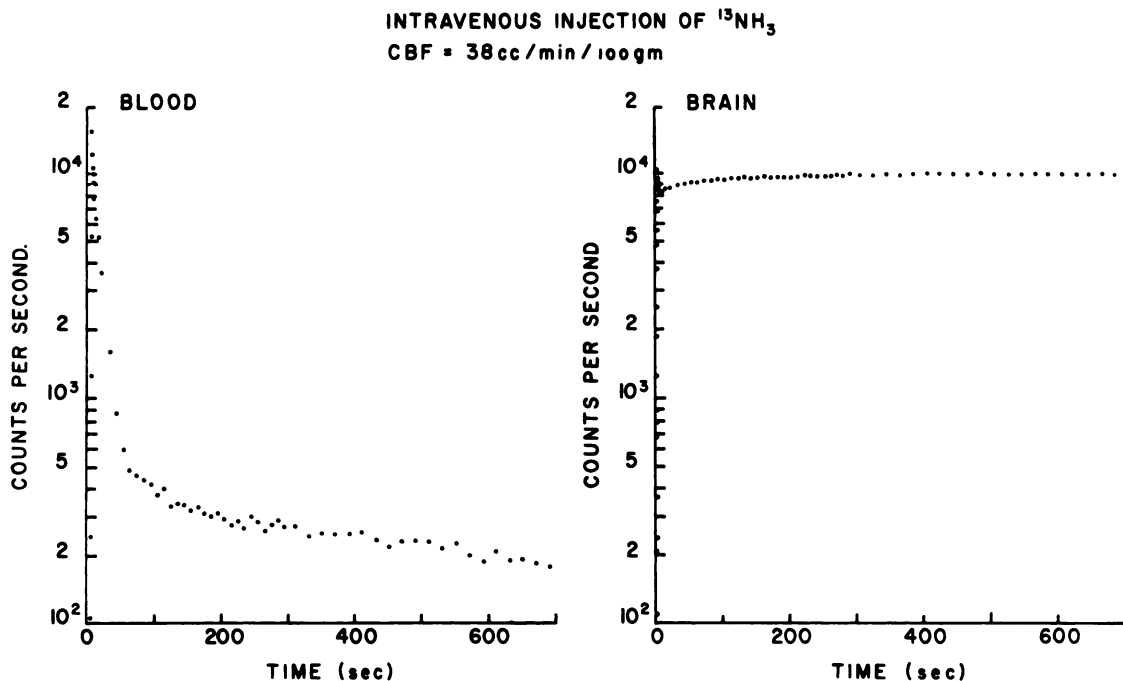

FIG. 3. Time–activity curves from blood and head after intravenous injection of $^{13}NH_3$ in rhesus monkey.

dure (Fig. 1) is due mainly to the dispersion of the $^{13}NH_3$ throughout the body circulation after the intravenous administration. Figure 3 shows that $^{13}NH_3$ clears rapidly from the blood: at 200 sec it is reduced to about 1.4% of the initial value. Thus, the
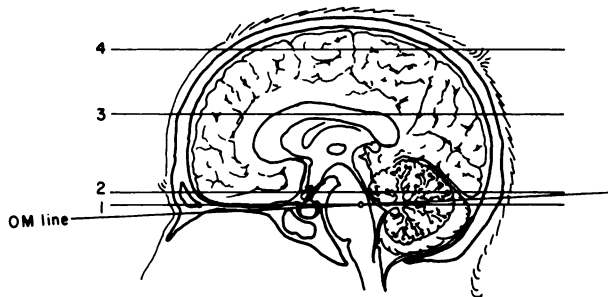

FIG. 4. Lateral view of head, indicating positions of cross-sectional levels in Fig. 5.
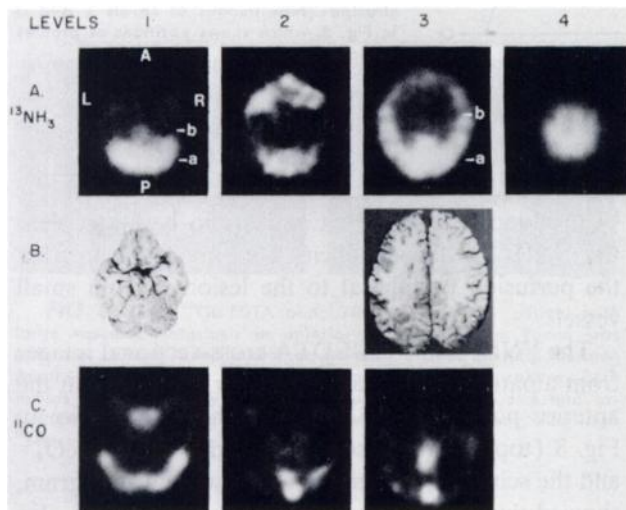

FIG. 5. Tomographic brain images of normal human volunteer following intravenous injection of $^{13}NH_3$ and inhalation of ^{11}CO. (A) Level 1 at orbital meatus (O.M.). High $^{13}NH_3$ accumulation is seen posteriorly in region of cerebellum and vermis. High $^{13}NH_3$ uptake just anterior to this region is probably due to brain stem. General variation due to cortex and white matter are also seen. Level 2 is about 1.5 cm above Level 1. Again, high uptake is noted posteriorly in cerebellum (which appears smaller at this level) and vermis. High uptake anteriorly is probably due to lowest portion of frontal lobe cortex. Level 3 is about 7 cm above O.M. and shows high uptake of $^{13}NH_3$ in cortex but little uptake in subcortical white matter. Level 4 is at top of brain and shows high $^{13}NH_3$ uptake in cortex. (B) Photographs of brain slices approximately at Levels 1 and 3. Brain slice for Level 1 is probably slightly above actual $^{13}NH_3$ image of Level 1 and slightly below $^{13}NH_3$ Level 2. (C) Blood pool distribution (^{11}CO-hemoglobin). Level 1 posteriorly shows transverse sinus (with normally dominant right side). Cavernous sinus and internal carotids are seen anteriorly. Increased blood content in area of sylvian fissure and cortex are noted. Level 2 posteriorly shows superior saggital sinus (SSS), straight sinus (SS), and part of the transverse sinus. Blood distribution in region of basal ganglia, sylvian fissure, and cortex are also seen. Level 3 shows prominent vascular structures of SSS and general vascular distribution of gray and white matter. Levels are tilted about 10° to O.M. line (see Fig. 5). Slice thickness and cross-sectional resolution are approximately 1.3 cm.

injected $^{13}NH_3$ will (A) distribute through the tissue with the flowing blood, (B) be extracted from the blood into the tissue, and (C) be retained in the large amino acid pool with a slow half-time of clearance back into the blood. Therefore, it may be possible to use $^{13}NH_3$ to image the blood perfusion distribution in the brain.

A series of normal human subjects were studied with the PETT III at a spatial resolution of 1.3 cm FWHM. Reconstructed tomographic images of $^{13}NH_3$ distribution were made at four levels (Fig. 4), ranging from the orbital meatus (O.M.) plane to the top of the brain. Figure 5 shows photographs of brain slices approximately corresponding to Levels 1 and 3. These slices were tilted about 10° with respect to the O.M. plane. Count profiles across the reconstructed $^{13}NH_3$ images, at the level of the O.M. and at 7 cm above the O.M., are shown in Fig. 6. At the lowest level (Level 1, Fig. 5A), the highest $^{13}NH_3$ uptake is in the region of the cerebellar hemispheres and vermis. The increased uptake just anterior to this region is probably due to the brain stem. The increased uptake of $^{13}NH_3$ in these structures is consistent with their greater portion of gray matter with its generous blood supply. The ratios of $^{13}NH_3$ uptake in (A) the cerebellar hemispheres and (B) the brain stem to that in the subcortical white matter, calculated from the numerical printout of the image, were found to be about 3.3 and 2.3, respectively (Fig. 6). If one assumes that the ratio of perfusion is equal to the ratio of capillary densities in different portions of the brain and that the cerebellum is 55% gray matter and 45% white matter (31), then the histologic work of Lierse and Horstmann (32) would indicate that the ratio of perfusion between the cerebellum and subcortical white matter is about 3.6. This agrees well with the maximum $^{13}NH_3$ ratio of 3.3 found for these regions, especially since the spatial resolution of PETT III causes some averaging of neighboring tissue, with a resultant lowering of the true uptake ratios. The average CBF ratio in cerebellum to subcortical white matter, using the autoradiographic studies in the cat by Landau et al (33) and Reivich et al (34), was calculated to be about 2.9. This value is somewhat lower than the human uptake ratio for $^{13}NH_3$ in these structures. At the level 7 cm above the O.M., the ratio of $^{13}NH_3$ in the cortex to the subcortical white matter varies from 3 posteriorly to about 2.5 anteriorly, which is consistent with the normal ratio of human capillary densities in these tissues of 3 (32). Here again the measured CBF ratio in the cat of 4.8, given by Landau et al (33) and Reivich et al (34) for these structures, does not agree with our $^{13}NH_3$ uptake as well as did the capillary density ratio.
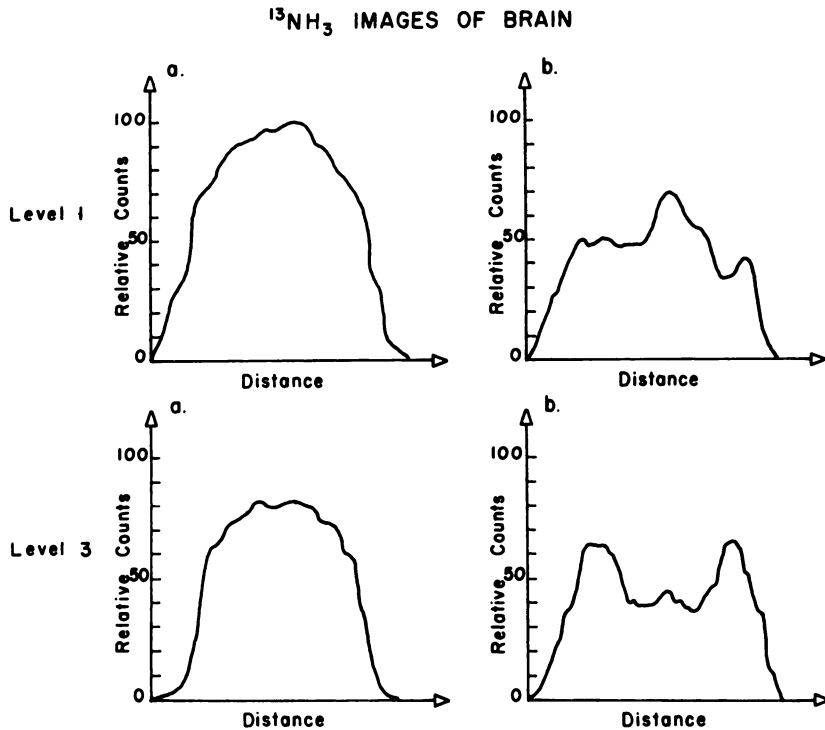
$^{13}NH_3$ IMAGES OF BRAIN

FIG. 6. Count profiles across reconstructed $^{13}NH_3$ images at Levels 1 and 3 in Fig. 5, which shows positions of profiles a and b.

Since the gray and white matter are intertwined in the region of the cerebral cortex (e.g., within the resolution capabilities of PETT III), the true ratio would be suppressed, making it difficult to discern whether the $^{13}NH_3$ uptake is better related directly to capillary density or to CBF. However, the CBF ratio (33,34) of cerebellum to subcortical white matter is lower than the $^{13}NH_3$ ratio, while the capillary density ratio is higher than the $^{13}NH_3$ uptake ratio. These results may indicate that the $^{13}NH_3$ uptake is more directly related to capillary density. There is also the question of species difference, since the $^{13}NH_3$ uptake and capillary density (32) measurements were performed in man, whereas the CBF distribution was for the cat (33,34).

The corresponding levels were also imaged with ^{11}CO-hemoglobin (Fig. 5C). The blood content of the large vessels dominates these images and somewhat obscures the blood content of the tissues. In comparison, $^{13}NH_3$ diffuses from the blood into the tissue through the large surface area and thin walls of the capillaries. Thus, the ^{11}CO-hemoglobin image shows the cross-sectional distribution of blood weighted by the volume of blood in all the vessels within the slice, whereas the $^{13}NH_3$ image is probably weighted by the distribution of capillary perfusion. The combined ^{11}CO and $^{13}NH_3$ study provides, in some cases, a means of distinguishing between large- and small-vessel involvement in lesions of the brain. For example, an arteriovenous malformation (non-nutrient flow) should show a high value in the ^{11}CO

image but no correspondingly high value on the $^{13}NH_3$ perfusion image (nutrient flow).

Figure 7 is from a stroke patient in whom the ^{11}CO blood-volume deficit appears to be larger than the $^{13}NH_3$ perfusion deficit. This may indicate that the perfusion peripheral to the lesion is from small vessels.

The $^{13}NH_3$ and ^{68}Ga-EDTA cross-sectional images from a patient with a large vascular metastasis in the anterior portion of the left hemisphere are shown in Fig. 8 (top). A rapid-sequence study with ^{99m}TcO$_4$^- and the scintillation camera, and also an arteriogram, showed this lesion to be highly vascular. This is also consistent with the high uptake of the $^{13}NH_3$, which had a ratio of 3 between the lesion and the same region in the contralateral hemisphere. There also
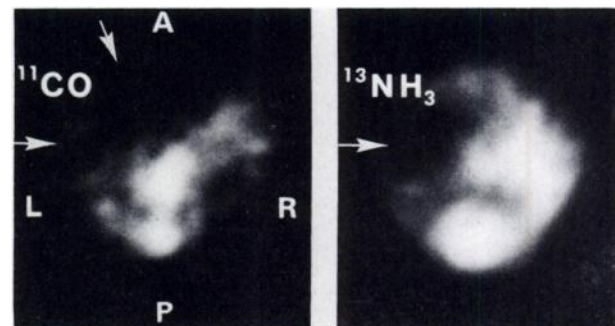

FIG. 7. $^{13}NH_3$ and ^{11}CO images of patient with stroke involving anterior region of left hemisphere. Note large involvement of blood volume deficit relative to perfusion. Spatial resolution in this study was about 2.2 cm.
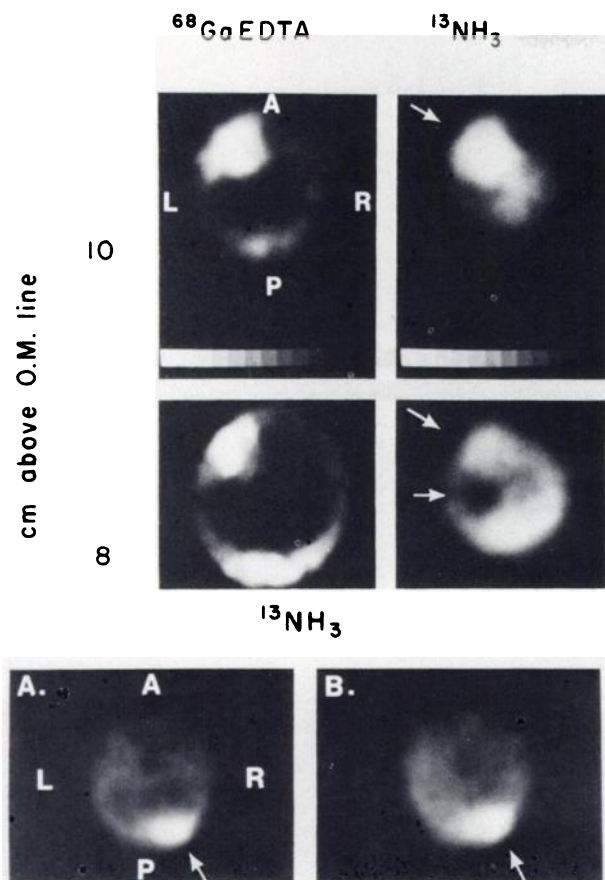
FIG. 8. (Top) ^{68}Ga-EDTA and ^{13}NH$_3$ images from patient with large vascular metastasis in anterior left hemisphere. Tumor was apparent in both levels examined (levels indicated at left). (Bottom) Another patient with tumor in posterior right hemisphere. Both tumors were shown by rapid-sequence radioactive studies and arteriography to be highly perfused, which is consistent with high ^{13}NH$_3$ uptake. Resolution was 2.2 cm.

appeared to be abnormally low perfusion posterior to the lesion at the level of 8 cm above the O.M. (Fig. 8, top). This could be a result of a low perfusion resistance in the vessels of the lesion compared to the surrounding tissue which results in theft of the blood flow from the surrounding tissue (the "steal phenomenon"). The abnormal accumulation of ^{68}Ga-EDTA shows the breakdown of the brain–blood barrier in the lesion. Another vascular metastasis is shown in Fig. 8 (bottom). This patient had a previous colectomy for carcinoma and presented with a left homonymous hemianopsia. Clinically the differential diagnosis included an occipital metastasis or a posterior cerebral artery infarction. The ^{13}NH$_3$ images showed an area of increased perfusion in the right occipital area, thus arguing against vascular occlusion. Subsequent neuroradiologic evaluation confirmed the metastasis.

In the patient studies presented (Figs. 7 and 8), the spatial resolution of the PETT III was reduced to 2.2 cm FWHM to provide higher detection effi-

ciency, since our present ^{68}Ge–^{68}Ga generator is capable of producing only about 3 mCi of ^{68}Ga. This lowered resolution produced a corresponding loss in image quality compared to the previous studies using 1.3 cm FWHM (e.g., Fig. 5).

Heart. The single-pass extraction of ^{13}NH$_3$ by the myocardium has also been studied by residue detection with the isolated perfused rat heart (Jones and Welch, unpublished data). The time–activity curves are very similar to those obtained in the brain, with the exception that the fraction of ^{13}NH$_3$ extracted by the heart is somewhat higher than that for the brain at comparable blood flows. Harper et al (7) reported that the first-pass extraction of ^{13}NH$_3$ in the myocardium of the dog was 90%. Hunter et al (36) suggested that ^{13}NH$_4^+$ acted as an analog of K^+. However, Hunter (37) and Harper et al (7) found that after administration of L-methionine-DL-sulfoximine [which is reported to inhibit the action of glutamine synthetase (38)], the uptake of ^{13}NH$_3$ was greatly reduced, indicating that normally NH$_3$ would be incorporated into the metabolism of glutamine in the heart. This is supported by the fact that there are large pools of glutamine and glutamic acid in the myocardium (39). This mechanism of ^{13}NH$_3$ uptake was confirmed (35) by chromatographic analysis of the effluent from an isolated perfused rat heart subsequent to the injection of ^{13}NH$_3$: the ^{13}N activity clearing from the heart was shown to be predominantly ^{13}N-glutamine. These findings are consistent with the work of Duda and Handler (40) in which the intravenous administration of ^{15}N-ammonium lactate in the rat produced ^{15}N-glutamine in the myocardium. Davidson and Sonnenblick (41), using an isolated perfused rat heart, also found that perfusing the heart with increasing concentrations of ammonium chloride (0.53–2.06 M) produced increasing levels of myocardial glutamine and increasing levels of glutamine in the effluent. Thus, the mechanism for ^{13}NH$_3$ retention in the myocardium appears to be the same as discussed above for the brain, and ^{13}NH$_3$ images of the myocardium should predominantly reflect the distribution of perfusion.

To evaluate the usefulness of ^{13}NH$_3$ and ^{11}CO-hemoglobin for myocardial imaging, six human volunteers and a patient with a myocardial infarct were studied with PETT III. Figure 9 shows the ^{13}NH$_3$ perfusion and ^{11}CO-hemoglobin blood-pool images from a normal subject at five different cross-sectional levels of the heart. The ^{13}NH$_3$ images show accumulation primarily within the left ventricular myocardium with some delineation of activity in the right ventricular wall (e.g., see Level C). The ^{11}CO-hemoglobin images show blood pools within the ventricu-
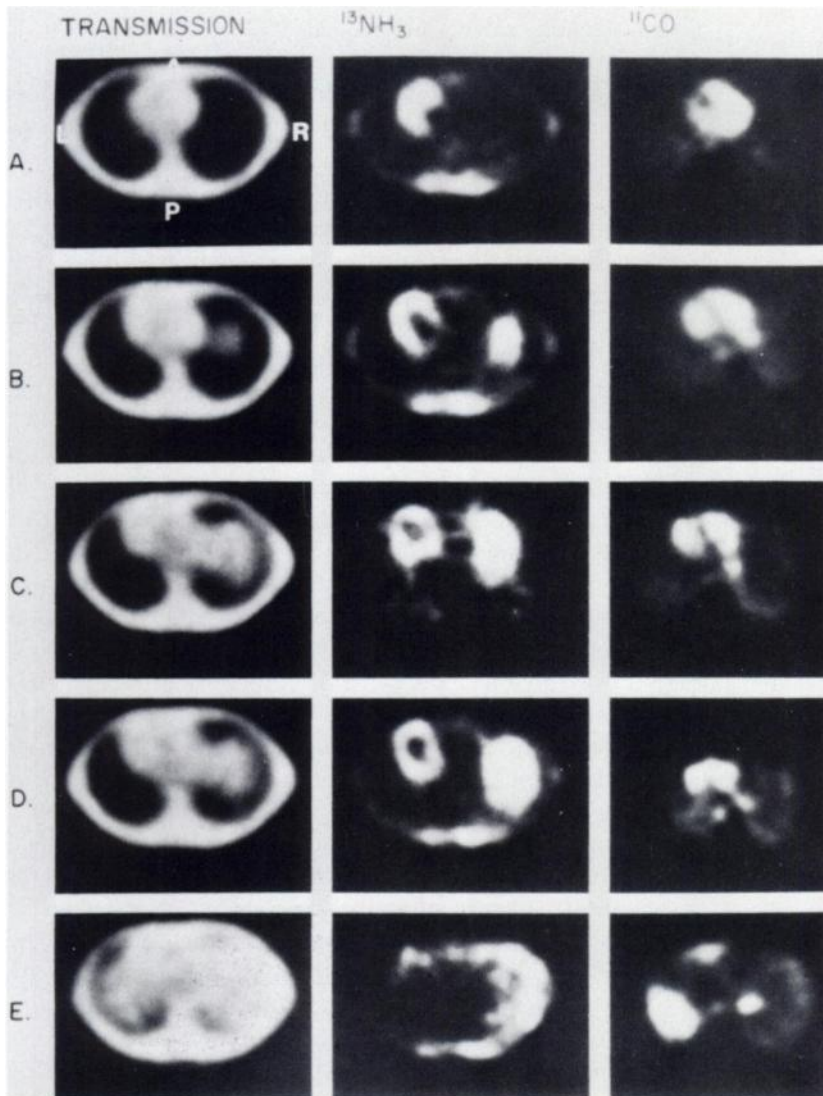
FIG. 9. Normal cardiac study for perfusion (^{13}NH$_3$) and blood pool (^{11}CO). Image was gated to include entire diastolic phase. Five cross-sectional levels are separated by about 1.5 cm, from superior (A) to inferior (E). (A) Left ventricle at this level appears as C-shaped area on ^{13}NH$_3$ study. ^{11}CO-hemoglobin image shows blood pool in left and right ventricular chambers. (B) Left ventricle appears as "horseshoe" on perfusion image and blood pool shows separation of left and right ventricles as well as right atrium. (C) Left ventricle shows as complete "ring" on ^{13}NH$_3$ image; note thinness of normal apical myocardium. ^{11}CO-hemoglobin images again shows left ventricular, right ventricular, and right atrial blood pool. (D) Left ventricle shows as "ring" in ^{13}NH$_3$ perfusion image; ^{11}CO-hemoglobin image shows cardiac blood pool as in (C) above and aorta posterior to heart. (E) ^{13}NH$_3$ accumulates at inferior tip of myocardium and in liver; high ^{13}NH$_3$ uptake posteriorly is in paraspinal muscles. ^{11}CO-hemoglobin shows inferior tip of left ventricle, spleen, and abdominal vessels.

Transmission images consist of reconstructed cross-sectional distribution of attenuation coefficients measured with external source of positron activity and PETT III. Transmission image shows anatomic cross section. Spatial resolution was 1.2 cm.

lar chambers. The interventricular septum is clearly defined.

A patient who had a recent anterior myocardial infarction was imaged with ^{13}NH$_3$ (Fig. 10). A large perfusion defect and apparent hypertrophy of the left ventricular wall is seen in the image.

Since it seems likely that an ischemic zone persisting for as long as 24 hr (as in this case) is tantamount to myocardial infarction, the image probably depicts a transmural infarction, shown as a zone of diminished ^{13}NH$_3$ accumulation resulting from diminished perfusion similar to that shown in the brain. Thus, tomographic reconstruction can help to elucidate the location and extent of myocardial ischemia in vivo.

CONCLUSION

The effective combination of positron transaxial tomography and the positron-emitting tracers ^{11}CO-

hemoglobin and ^{13}NH$_3$ provide a clinically safe method for producing high-quality tomographic images of vascular volume and blood perfusion in the brain and heart. The resulting images exhibit high
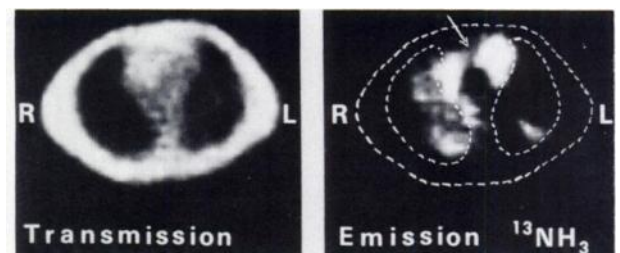

FIG. 10. Patient (weight 265 lb) with transmural anterior myocardial infarct. ^{13}NH$_3$ perfusion image shows large area of absent activity (perfusion defect) in anterior myocardium, extending through myocardium. No cardiac gating was employed. Transmission image shows anatomic distribution in examined cross section. Spatial resolution was 2.2 cm FWHM.

spatial resolution in all three dimensions and quantitative accuracy both in a relative and absolute manner. The quantitative feature of the tomographic procedures yields images with high image contrast; if the region of interest is 2–3 times greater than the sampling interval, then image contrast equals object contrast. It also provides a means of carrying out quantitative physiologic studies.

The tracer $^{13}NH_3$ is excellent for imaging the distribution of tissue perfusion. It distributes throughout the tissue with the flowing blood, diffuses from the blood into the tissue through the capillary surfaces used for nutrient exchange, and is retained in the tissue with a very slow return from tissue back to blood (from an intravenous injection the tissue clearance half-time is approximately 60–70 min). Thus, $^{13}NH_3$ appears to behave like an ideal tracer for static blood flow or perfusion imaging. The ^{11}CO-hemoglobin and $^{13}NH_3$ images also provide important diagnostic information since the former is weighted by the volume of blood in vessels of all sizes and the latter reflects the extent of capillary perfusion. The avoidance of superposition of structures by the tomographic reconstruction removes the difficulties resulting from interfering activity surrounding the organ (or region) of interest, which in the past has limited the interpretation of data from intravenous injection techniques.

The advantages that transaxial tomography have brought to x-ray transmission are also possible for radionuclide imaging. An important difference in these two techniques resides in the capability of radionuclide tomography to provide images that represent physiologic functions of the organ. A major factor in the full realization of this goal rests in the selection of labeled compounds whose chemical or physiologic properties are not significantly perturbed by the addition of the radionuclide to the selected compound. The positron-emitters ^{11}C, ^{13}N, and ^{15}O undeniably and uniquely fulfill this requirement. However, it should also be mentioned that in some cases physiologic functions can be studied with labeled analogs. Properly chosen analogs may even simplify the interpretation of the results. For example, labeled 2-deoxyglucose can be substituted for glucose in cerebral metabolism studies with the added advantage that, while its transport is like that of glucose, its metabolic activity stops once it enters the cells and is phosphorylated (42). Thus, one avoids the complicating release of breakdown products back into the blood stream (43). The positron-emitters ^{18}F, ^{68}Ga (from a commercial generator system of ^{68}Ge), ^{82}Rb (from a generator system of ^{82}Sr), and ^{54}Co can be used to label many compounds currently used in nuclear medicine or to label analogs. These radionuclides together provide a broad base for the innovative development of new radionuclide imaging procedures.

REFERENCES

1. ZIERLER KL: Equations for measuring blood flow by external monitoring of radioisotopes. Circ Res 16: 309–321, 1965
2. SAPERSTEIN LW: Regional flow by fractional distribution of indicators. Am J Physiol 193: 161–168, 1958
3. PHELPS ME, HOFFMAN EJ, MULLANI NA, et al: Transaxial emission reconstruction tomography: Coincidence detection of positron-emitting radionuclides. In Noninvasive Brain Imaging, Computed Tomography and Radionuclides, DeBlanc H, Sorenson JA, eds. New York, Society of Nuclear Medicine, 1975, pp 87–110; Phelps ME: Computerized transaxial tomography: Transmission and emission. Paper given at the Planery Session of the 21st Annual Meeting of the Society of Nuclear Medicine, San Diego, 1974
4. KUHL DE, REIVICH M, ALAVI A, et al: Local cerebral blood volume determined by three-dimensional reconstruction of radionuclide scan data. Circ Res 36: 610–619, 1975
5. BUDINGER TF, DeLAND FH, DUGGAN HE, et al: Dynamic time-dependent analysis and static three-dimensional imaging procedures for computer-assisted CNS studies. In Noninvasive Brain Imaging, Computer Tomography and Radionuclides, DeBlanc H, Sorenson JA, eds. New York, Society of Nuclear Medicine, 1975, pp 45–66
6. HARPER PV, LATHROP KA, KRIZEK H, et al: Clinical feasibility of myocardial imaging with $^{13}NH_3$. J Nucl Med 13: 278–280, 1972
7. HARPER PV, SCHWARTZ J, BECK RN, et al: Clinical myocardial imaging with nitrogen-13 ammonia. Radiology 108: 613–617, 1973
8. MONAHAN WG, TILBURY RS, LAUGHLIN JS: Uptake of ^{13}N-labeled ammonia. J Nucl Med 13: 274–277, 1972
9. HOOP B, SMITH TW, BURNHAM CA, et al: Myocardial imaging with $^{13}NH_3$ and a multicrystal positron camera. J Nucl Med 14: 181, 1973
10. HOOP B, HNATOWICH JD, BROWNELL GL, et al: Techniques for positron scintigraphy in the brain. J Nucl Med 17: 473–479, 1976
11. BROWNELL GL, BURNHAM CA, CHESLER DA, et al: Transverse section imaging of radionuclide distributions in heart, lung and brain. In Reconstruction Tomography in Diagnostic Radiology and Nuclear Medicine, Ter-Pogossian MM, Phelps ME, Brownell GH, et al, eds. Baltimore, Md., University Park Press: to be published
12. BUDINGER TF, YANO Y, HOOP B: A comparison of $^{82}Rb^+$ and $^{13}NH_3$ for myocardial positron scintigraphy. J Nucl Med 16: 429–431, 1975
13. CARTER CC, LIFTON JF, WELCH MJ: Organ uptake and blood pH and concentration effects of ammonia in dogs determined with ammonia labeled with 10 minute half-lived nitrogen-13. Neurology 23: 204–213, 1973

14. KUHL DE, EDWARDS RQ: The Mark IV system for emission computerized tomography and quantitative reconstruction of brain radioactivity. *J Nucl Med* 16: 543, 1975

15. BUDINGER TF: Private communication

16. PHELPS ME, HOFFMAN EJ, MULLANI NA, et al: Application of annihilation coincidence detection to transaxial reconstruction tomography. *J Nucl Med* 16: 210–224, 1975

17. TER-POGOSSIAN MM, PHELPS ME, HOFFMAN EJ, et al: A positron emission transaxial tomograph for nuclear medicine imaging (PETT). *Radiology* 114: 89–98, 1975

18. PHELPS ME, HOFFMAN EJ, COBLE CS, et al: Performance and design characteristics of PETT III. In *Reconstruction Tomography in Diagnostic Radiology and Nuclear Medicine*, Ter-Pogossian MM, Phelps ME, Brownell GH, et al, eds. Baltimore, Md., University Park Press: to be published

19. TER-POGOSSIAN MM, PHELPS ME, HOFFMAN EJ, et al: Performance characteristics of a positron transaxial tomograph (PETT III). In *Reconstruction Tomography in Diagnostic Radiology and Nuclear Medicine*, Ter-Pogossian MM, Phelps ME, Brownell GH, et al, eds. Baltimore, Md., University Park Press: to be published

20. TER-POGOSSIAN MM, PHELPS ME, HOFFMAN EJ, et al: A positron emission transaxial tomograph (PETT) for the three-dimensional and non-invasive measure of cerebral hemodynamics and metabolism. *Seventh International Symposium on Circulation and Metabolism*, Harper AM, Rowan JO, et al, eds. To be published

21. PHELPS ME, TER-POGOSSIAN MM, HOFFMAN EJ, et al: A computerized transaxial tomograph for nuclear medicine imaging. *J Nucl Med* 16: 558, 1975

22. COLEMAN RE, HOFFMAN EJ, PHELPS ME, et al: Application of computerized radionuclide transaxial tomography with positron emitting radiopharmaceuticals. *J Nucl Med* 16: 521, 1975

23. TER-POGOSSIAN MM, HOFFMAN EJ, WEISS ES, et al: Positron emission reconstruction tomography for the assessment of regional myocardial metabolism by the administration of substrates labeled with cyclotron-produced radionuclides. In *Cardiovascular Imaging and Image Processing: Ultrasound, Angiography and Isotopes*. Stanford, Calif., Stanford University Press: to be published

24. HOFFMAN EJ, PHELPS ME, MULLANI NA, et al: Design and performance characteristics of a whole-body positron transaxial tomograph. *J Nucl Med* 17: 493–502, 1976

25. TILBURY RS, DAHL JR, MONAHAN WG, et al: The production of ¹³N-labeled ammonia for medical use. *Radiochem Radioanal Lett* 8: 317–323, 1971

26. STRAATMANN MG, WELCH MJ: Enzymatic synthesis of nitrogen-13 labeled amino acids. *Radiat Res* 56: 48–56, 1973

27. EICHLING JO, RAICHLE RE, GRUBB RL, et al: Evidence of the limitations of water as a freely diffusible tracer in brain of the rhesus monkey. *Circ Res* 35: 358–364, 1974

28. PHELPS ME, EICHLING JO: A quick method for calculation of the vascular mean transit time. *J Nucl Med* 15: 814–817, 1974

29. DANIELS F, ALBERTY RA: *Physical Chemistry*, 3rd ed. New York, Wiley, 1965, p 365

30. MCILLWAIN H: *Biochemistry and the Central Nervous System*, 3rd ed. Boston, Mass., Little, Brown, and Co., 1966, p 373

31. HOEDT-RASMUSSEN K: Regional cerebral blood flow. The intra-arterial injection method. *Acta Neurol Scand* 43: 1–81, 1967 (also see reference contained within)

32. LIERSE W, HORSTMANN E: Quantitative anatomy of the cerebral vascular bed with special emphasis on homogeneity and inhomogeneity in small parts of the grey and white matter. In *Regional Cerebral Blood Flow*, Ingvar DH, Lassen NA, eds. Copenhagen, Monksgaard, 1970, pp 15–19

33. LANDAU WM, GREYGANG WH, ROWLAND LP, et al: The local circulation of the living brain; values in the unanesthetized and anesthetized cat. *Trans Am Neurol Assoc* 80: 125–129, 1955

34. REIVICH M, JEHLE J, SOKOLOFF L, et al: Measurement of regional cerebral blood flow with antipyrine-¹⁴C in awake cats. *J Appl Physiol* 27: 296–300, 1969

35. JONES T, WELCH MJ: Unpublished data, 1973

36. HUNTER WW, MONAHAN WG: ¹³N-ammonia: A new physiological radiotracer for molecular medicine. *J Nucl Med* 12: 368, 1971

37. HUNTER WW: Presentation in discussion. In *IAEA Symposium on Medical Radioisotope Scintigraphy*. Vienna, IAEA, 1972, pp 23–28

38. RAO SLN, MEISTER A: In vivo formation of methionine sulfoxamine phosphate, a protein bound metabolite of methionine sulfoxamine. *Biochemistry* 11: 1123–1127, 1972

39. MORGAN HE, EARL DCN, BROADUS A, et al: Regulation of protein synthesis in heart muscle. I. Effect of amino acid levels on protein synthesis. *J Biol Chem* 232: 303–314, 1958

40. DUDA G, HANDLER P: Kinetics of ammonia metabolism in vivo. *J Biol Chem* 232: 303–314, 1958

41. DAVIDSON S, SONNENBLICK EH: Glutamine production by the isolated perfused rat heart during ammonium chloride perfusion. *Cardiovasc Res* 9: 295–301, 1975

42. REIVICH M: Personal communication, 1975

43. RAICHLE ME, LARSON KB, PHELPS ME, et al: In vivo measurement of brain glucose transport and metabolism employing glucose-¹¹C. *Am J Physiol* 228: 1936–1948, 1975